Engineering Failure Analysis 66 (2016) 373–384

Contents lists available at ScienceDirect

Engineering Failure Analysis

journal homepage: www.elsevier.com/locate/engfailanal

Interaction of hot corrosion and creep in Alloy 617

Amin Homaeian [a,*], Mostafa Alizadeh [b]

[a] Department of Materials Science and Engineering, Graduate University of Advanced Technology, P.O. Box: 76315-117, Kerman, Iran
[b] Department of Metals, Institute of Science and High Technology and Environmental Sciences, Graduate University of Advanced Technology, P.O. Box: 76315-117, Kerman, Iran

ARTICLE INFO

Article history:
Received 26 August 2015
Received in revised form 4 March 2016
Accepted 10 March 2016
Available online 12 March 2016

Keywords:
Alloy 617
Creep
Hot corrosion

ABSTRACT

In the present work, Alloy 617 was subjected to creep in the absence and presence of hot corrosion (i.e. with and without a deposit of sodium salts) under different load magnitudes at 850 °C. Additionally, a sample of the alloy was exposed to hot corrosion without applying creep. The results revealed that the creep behavior of Alloy 617 was substantially affected by hot corrosion which accelerated creep and led to a considerable reduction in the fracture ductility and creep life of the alloy. Microscopic examinations demonstrated that the strain-to-rupture decreased due mainly to the damage accumulation during tertiary creep. Various mechanisms of hot-corrosion/creep interaction were discussed that highlighted the destructive role of $M_{23}C_6$ precipitates in the interaction. It was explained that hot corrosion contributed to the reduction of grain-boundary cohesive-strength followed by extensive cavitation at transvers grain boundaries.

1. Introduction

Alloy 617 (UNS N06617) is a solid solution strengthened superalloy of Ni, Cr, Co and Mo. Owing to the unique metallurgical composition, Alloy 617 has great resistance to high temperature corrosion in various environments and has been developed for high temperature applications above 800 °C. Therefore, it is often considered as a candidate for applications in gas turbines and power generation structures, heat exchangers, chemical manufacturing components and metallurgical processing facilities [1]. In these cases, there are components which work under high pressure and temperature and consequently are susceptible to creep and also simultaneous hot corrosion due to the usage of low grade fossil fuels. Singh et al. [2] has carried out a comprehensive review and reported that some fuels such as coal and fuel oil, due to their impurities (e.g. Na, S and V), deposit an alkaline metal salt layer on hot components during combustion, which is corrosive and results in hot corrosion of the substrate.

Hot corrosion and creep have synergistic effects on each other, and their interaction leads to the premature failure of alloys [2,3]. These two destructive phenomena have been investigated separately in several studies, but usually without taking their interaction into consideration. In order to study the interaction of hot corrosion and creep experimentally creep specimens are either coated with a salt deposit, as done by Ref. [4–6], or exposed to corrosive atmosphere, as tested by Ref. [7]. Lin et al. [4] investigated the creep behavior of Alloy GH-37 coated with Na_2SO_4 — 25 wt.% NaCl at 700 and 850 °C. They observed that hot corrosion decreases the creep life and fracture ductility of the alloy. Likewise, Suryanarayanan et al. [5] tested 304 stainless steel in the temperature range of 600–700 °C and reported that the eutectic liquid phase Ni-Ni_3S_2 formed in salt penetrated into grain boundaries and reduced the creep life. Yoshiba [6] coated Alloy 751 with Na_2SO_4 — 10 wt.% NaCl and conducted the creep tests at 800 °C with controlling the oxygen partial pressure. He remarked that creep forms micro-channels in the oxide scale and grain boundaries through which the molten salt directly penetrated along grain boundaries.

* Corresponding author.
E-mail address: amin.homaeian@gmail.com (A. Homaeian).

http://dx.doi.org/10.1016/j.engfailanal.2016.03.012
1350-6307/

Table 1
Chemical composition of Alloy 617 used in the study.

Element	C	Mn	Fe	Si	Cu	Cr	Ni	Al	Ti	Co	Mo	V	Nb	Zr	W	S
wt.%	0.07	0.08	1.5	0.15	0.06	21.48	54.43	1.2	0.4	11.8	8.6	0.01	0.08	0.01	0.12	Trace

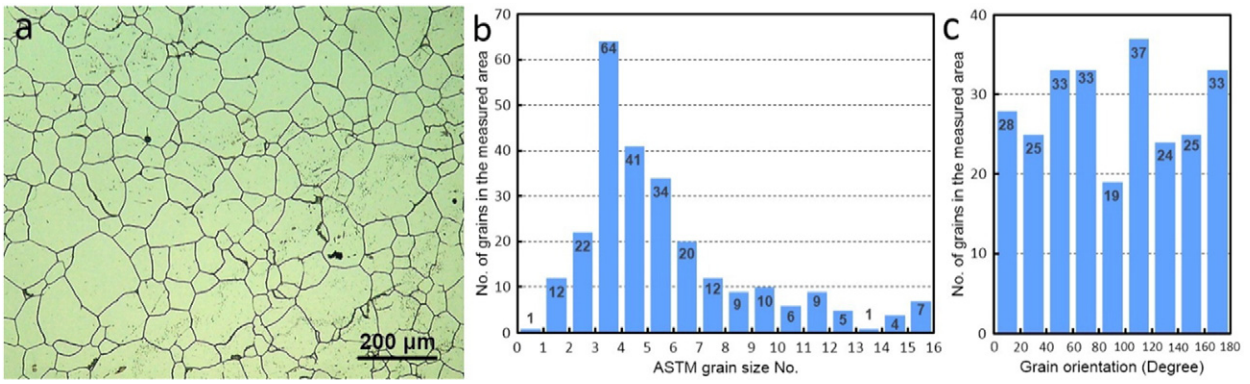

Fig. 1. As-received Alloy 617: (a) optical micrograph of the microstructure, (b) grain size distribution and (c) grain orientation in a (the measured area).

Combustion chambers of gas turbines work at high pressure and high temperature gas flow containing corrosive species and are consequently exposed to simultaneous hot corrosion and creep. Furthermore, combustion chamber walls are usually thin, which according to the result of Roy et al. [8] makes oxidation-creep interaction more effective. In the present work, an unused combustion chamber made of hot-rolled Alloy 617 sheet was selected as a sample to study the interaction. The purpose of this research is to evaluate the behavior of Alloy 617 under simultaneous hot corrosion and creep and to characterize the interaction mechanisms. This can provide a clear understanding of the failure under hot corrosion and creep and leads us into the solutions and also more accurate service-life prediction, matters of controversy in high-temperature applications.

2. Experimental procedure

The chemical composition of the sample sheet is given in Table 1.

Fig. 1a shows the microstructure of the as-received alloy. The grain size distribution in Fig. 1a, given in Fig. 1b, was measured according to ASTM E112-96. The corresponding grain orientation given in Fig. 1c shows that the grains were randomly oriented.

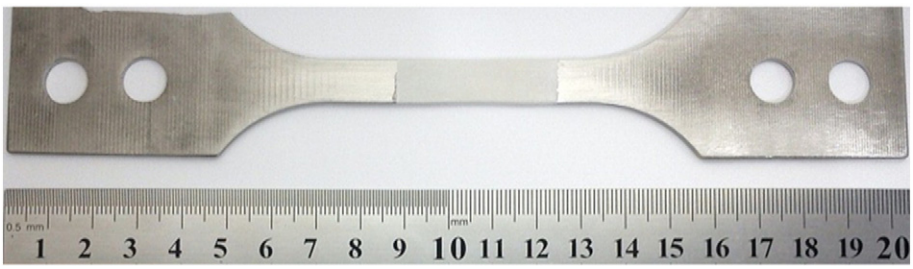

Fig. 2. The salt-coated creep specimen.

Table 2
Specimen IDs and the initial applied stress in creep tests.

Stress (MPa)	85	105	125
Salt coated	C1	C2	C3
Non coated	N1	N2	N3

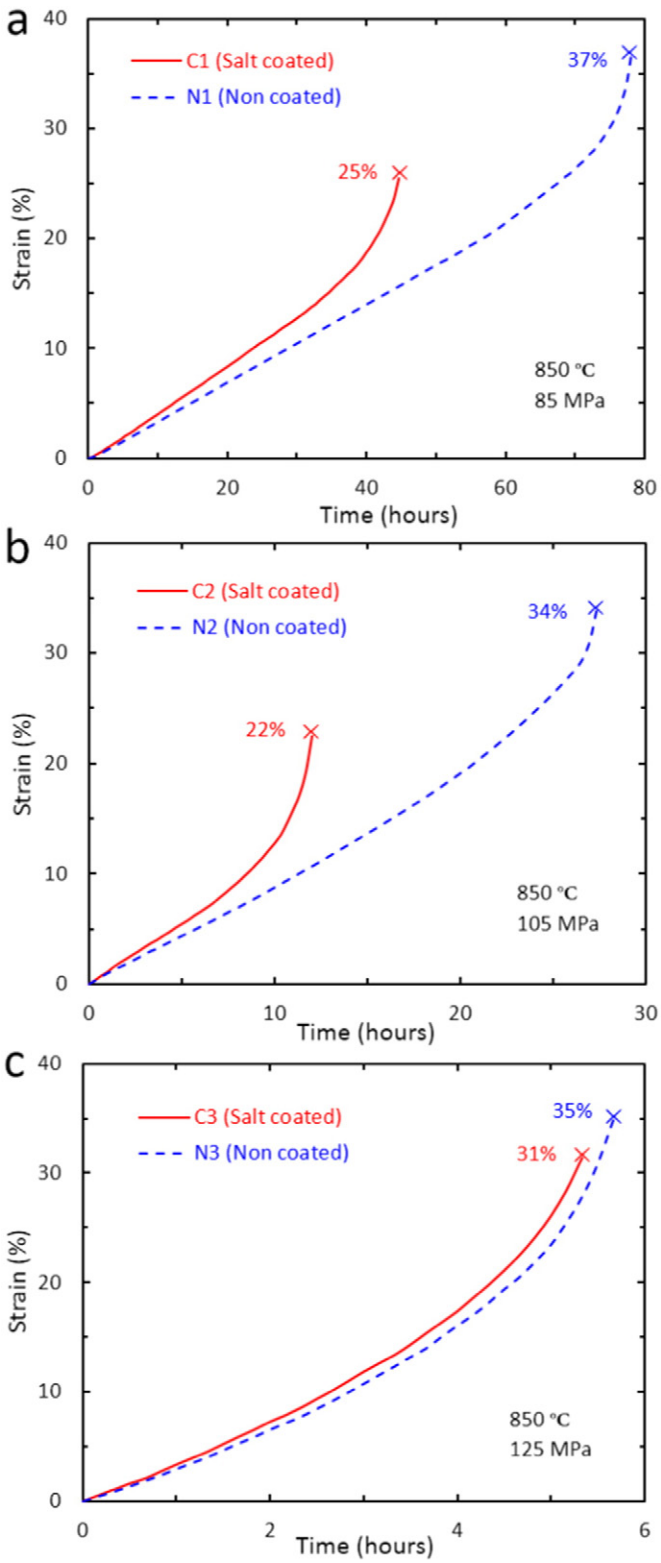

Fig. 3. Creep-rupture curves of Alloy 617.

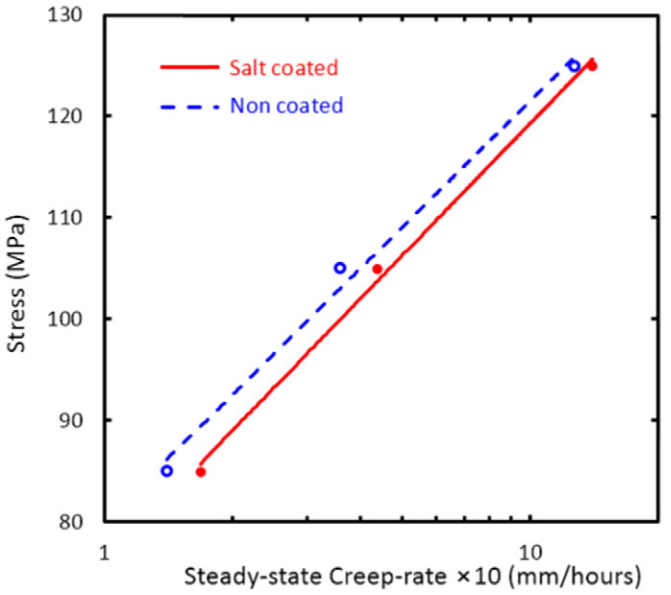

Fig. 4. Applied stress versus steady-state creep-rate.

No heat treatment was conducted in order to keep the as-received microstructure and to evaluate the practical microstructure of combustion chambers in the experiments.

Creep specimens with the gage dimensions of 40 mm × 10 mm × 1.7 mm were gently cut out from the sample sheet using a CNC wire-cut EDM (the specimen axis was parallel with the sheet rolling direction); afterwards, they were polished with SiC paper and degreased in ethanol-acetone mixture followed by cleaning in distilled water. In order to provide the hot corrosive conditions for the specimens at elevated temperature, they were coated on the gage with the synthetic salt mixture composed of Na_2SO_4 — 30 wt.% $NaVO_3$ — 10 wt.% NaCl, as shown in Fig. 2. The super saturated aqueous solution of the given salt mixture was prepared and applied on the specimens pre-heated up to 200 °C. The water content of the solution rapidly vaporized after applying the solution leaving a fairly compact deposit on the specimens. This process was repeated until the amount of the deposit was uniformly 30 mg/cm^2 on all of the specimens.

Table 2 shows the initial applied stress in creep tests and the specimen IDs that henceforth will be used to refer to the specimens. Creep-rupture tests were carried out under constant load at 850 °C. The specimens were heated up in the air using a split tube furnace. In addition, a rectangle-shaped specimen (referred to by *non-loaded specimen* in the text) was prepared and coated with salt, placed in the furnace and was heated up simultaneously with the creep test of C1.

The corrosion products, in the powder form, were identified by the X-ray diffraction. The crept specimens were initially examined using a stereo microscope, and C1 and N1 were selected for further examinations. The selected specimens were mounted with epoxy and polished with SiC paper grade 2400. The samples were then analyzed by optical and scanning electron microscopies. SEM-EDAX analysis of the alloy-oxide interface and cracks was also performed. In order to perform optical microscope analysis, the samples were finished with 0.25 μm diamond paste and etched in marble solution (4 g of 1 M $CuSO_4$ — 20 ml of 37% HCl — 20 ml H_2O).

3. Results and discussions

Fig. 3 shows the creep-rupture curves (strain versus creep time) for the salt-coated and non-coated specimens. Under three stresses, the salt coating led to an increase in the creep rate (the slope of curves) followed by a sharp decrease in the creep life (time-to-rupture) and fracture ductility (strain-to-rupture).

Table 3
Percentage of reduction in the cross-sectional area.

Specimen ID	Reduction in area (%)
C1	12.2
N1	19.3
C2	10.5
N2	16.7
C3	15.7
N3	15.9

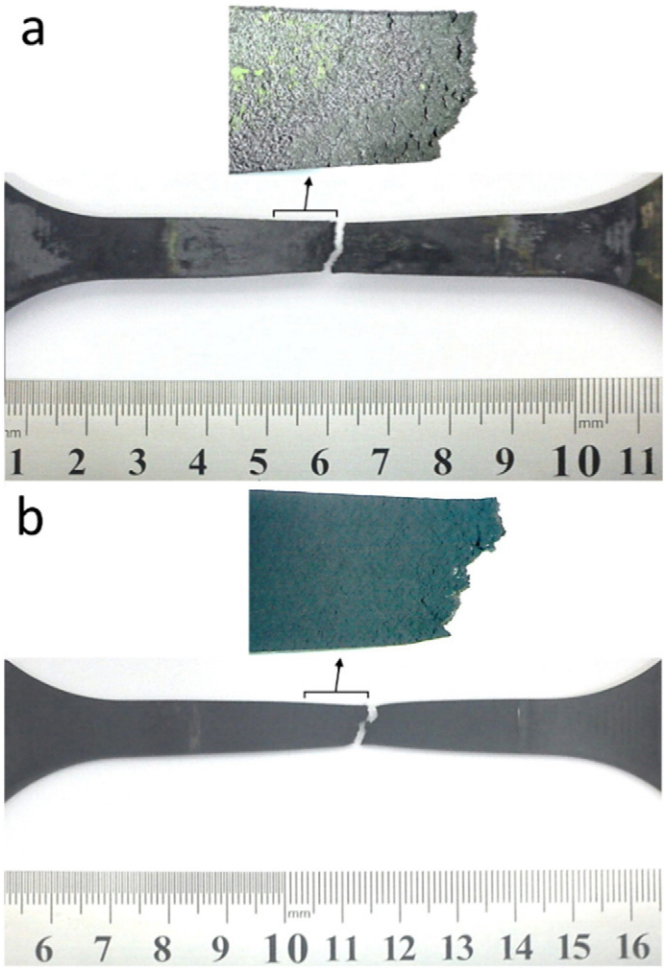

Fig. 5. Ruptured specimens (a) C1 and (b) N1.

Fig. 4 (extracted from Fig. 3) shows how hot corrosion increased the secondary creep-rate. This increase in secondary creep-rate is attributed to the slight reduction in the load bearing cross-sectional area of the creep specimens by hot corrosion, which leads the stress to increase. However, after final rupture, the reduction of area in the coated specimens was less than that of the non-coated specimens, as shown in Table 3. In other words, the coated specimens exhibited lower ductility compared to the non-coated specimens. Accordingly, the role of hot corrosion in reduction of cross section is dominated by other more effective phenomena that are discussed later in this article.

The ruptured specimens C1 and N1 are respectively shown in Fig. 5a and b. As indicated in the enlarged views of the gage near the ruptured zone, the corrosion-product scale on C1 was full of pores and cracks, whereas the oxide scale on N1 was uniform, compact and perfectly adherent.

The microstructure of the as-received alloy is shown in Fig. 6a. Various precipitates with different sizes can be observed in the as-received alloy; large primary carbides including Mo-rich M_6C and Ti-rich M(C, N) (indicated by number 1) and a great number of small Cr-rich $M_{23}C_6$ type carbides (indicated by number 2) were distributed within the austenitic grains and grain boundaries. Similar observations were reported by Chomette et al. [9].

As shown in Fig. 6b and c, creep of the specimen C1 generated twins, indicated by number 3. Additionally, after creep, the precipitates ($M_{23}C_6$ carbides in particular) were generated significantly at the grain boundaries. However, a considerable fraction of Mo-rich M_6C and Ti-rich M(C, N) were still present within the grains. This can be attributed to the larger size of these carbides and the lower diffusion coefficient of Mo compared to Cr in Ni with the FCC crystal structure [10].

As Fig. 6b and c depict the precipitates were mainly generated at the grain boundaries which were transverse to the tensile stress (loading direction). It is well known that Alloy 617 is generally susceptible to hot corrosion and oxidation around $M_{23}C_6$ carbides due to the low chromium concentration adjacent to these precipitates. Therefore, the intergranular carbides generated during creep cause hot corrosion to effectively attack the transverse grain boundaries, where creep largely takes effect; this facilitates the destructive interaction of hot corrosion and creep.

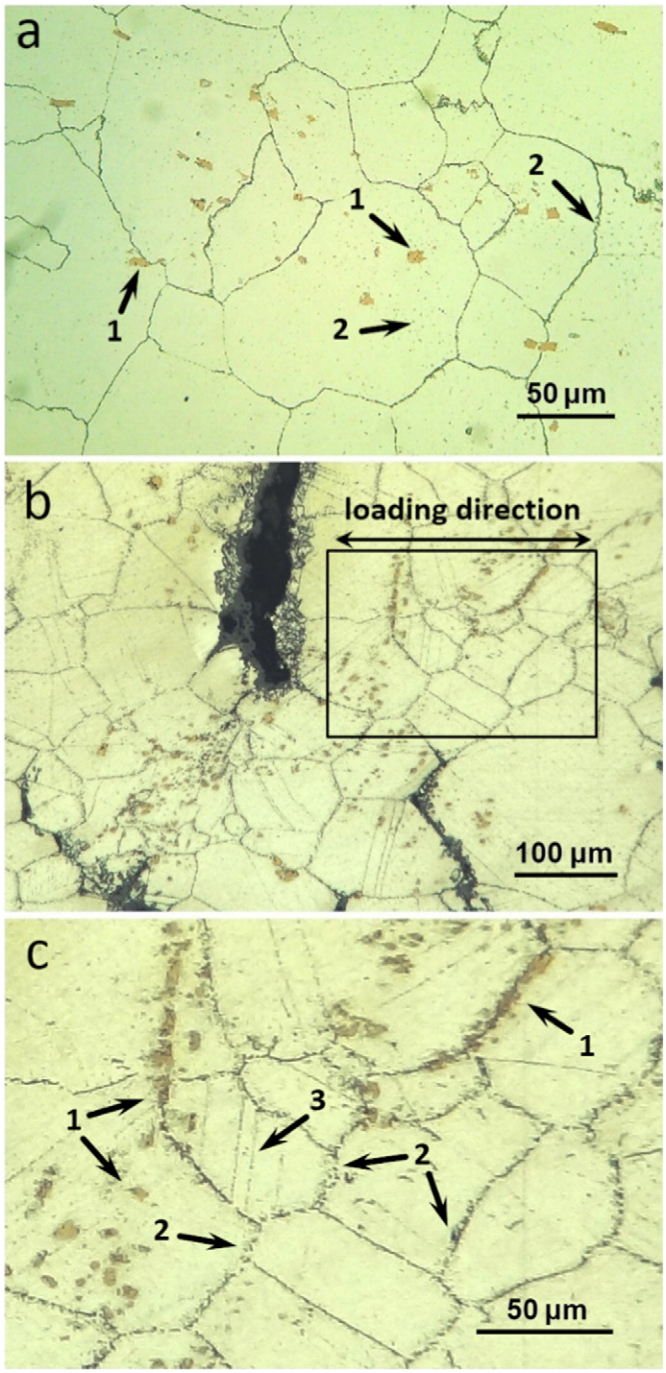

Fig. 6. Optical micrographs of (a) the as-received alloy, (b) the longitudinal section of C1 near the ruptured zone, (c) the larger view of the squared area in b, **1**: primary carbides; **2**: $M_{23}C_6$ carbides; **3**: twins.

The redistribution of $M_{23}C_6$ carbides discussed above and increase in the amount of carbides at grain boundaries during creep (compare Fig. 6a with 6c) are controlled by diffusion and occur through stress-assisted carbon diffusion from the carbides with less stability (due to their size and type) to the more stable carbide precipitates. The redistribution then contributes to the formation of a semi-continuous network of carbides which predisposes Alloy 617 to further intergranular corrosion.

Fig. 7a shows the section of the non-loaded hot corrosion specimen with the X-ray map of O, Ni, Cr and Co. The X-ray map reveals that hot corrosion formed a thick two-layered scale on the surface including a Cr–Co enriched inner layer as well as a Ni-rich outer layer. Similar morphology can be seen for scale on C1 in Fig. 7b and c, which means that the distribution of elements

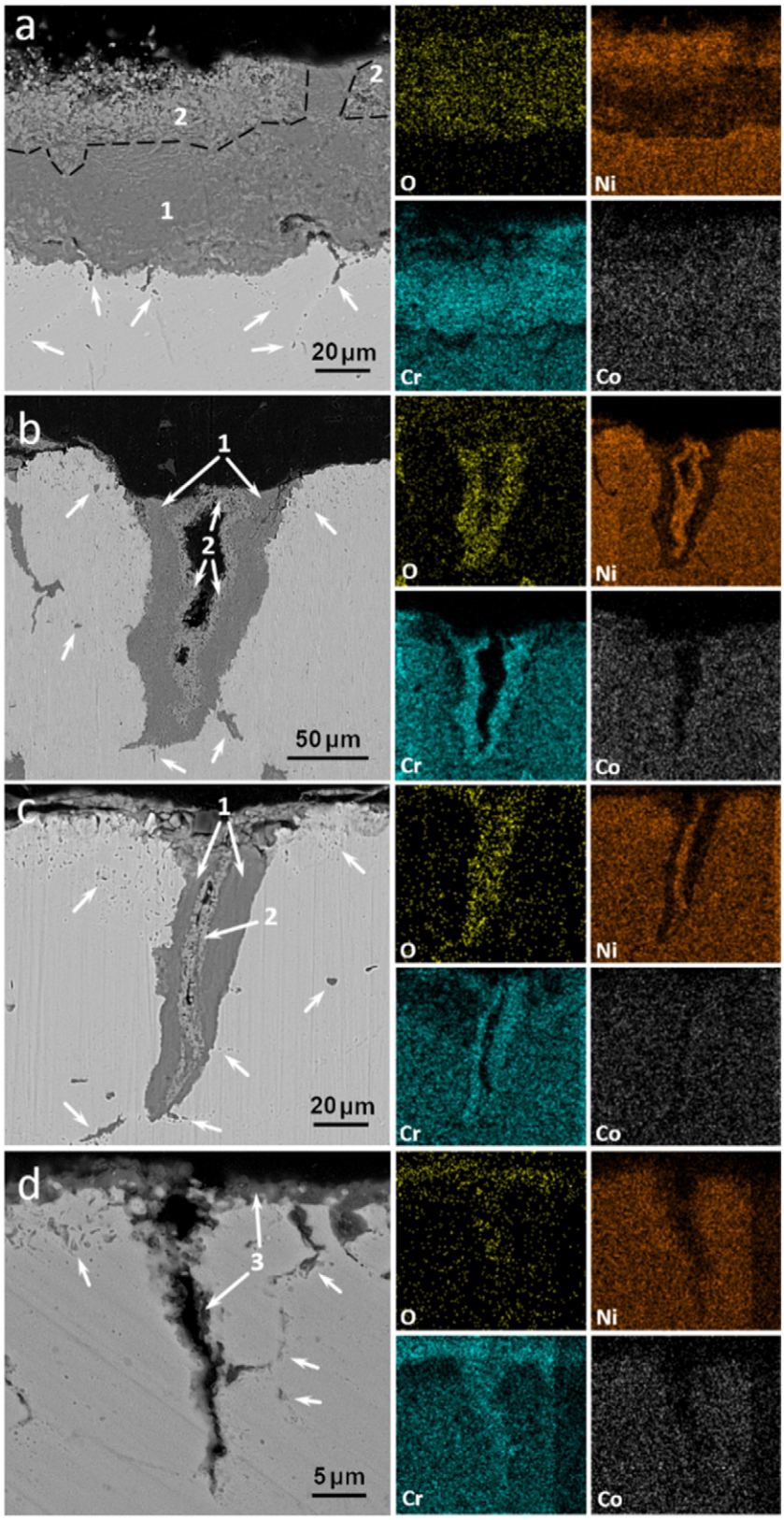

Fig. 7. Back-scattered electron images and the X-ray analysis of (a) non-loaded hot corrosion specimen, (b and c) C1 and (d) N1 near the ruptured zone, **1**: Cr-Co enriched inner layer; **2**: Ni-rich outer layer; **3**: Cr-rich oxide scale, arrows indicate intergranular oxides and voids.

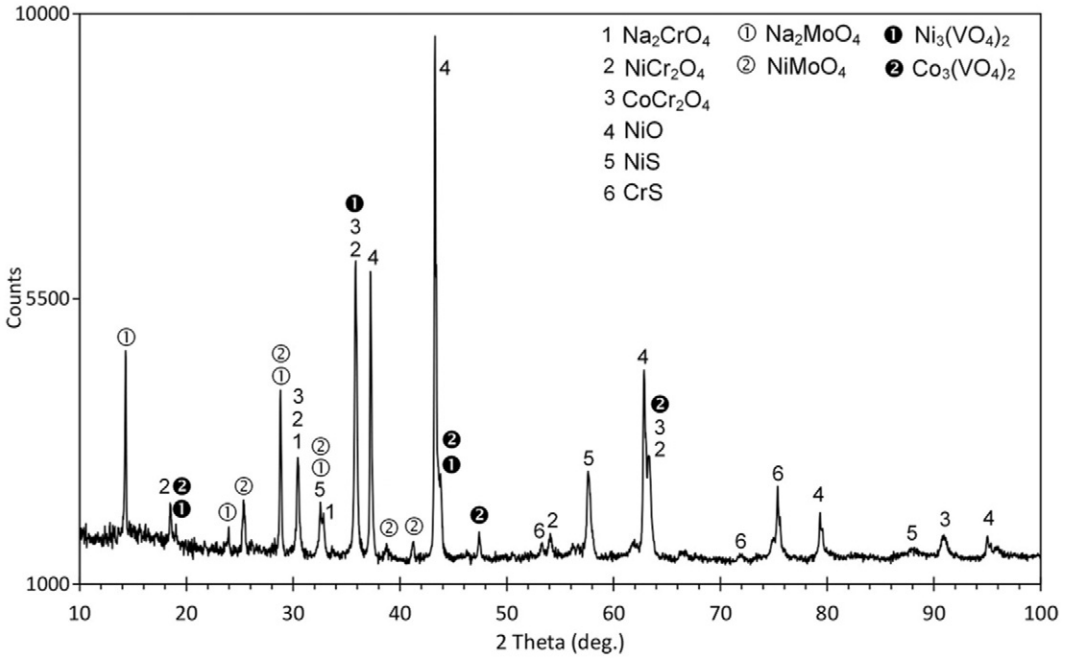

Fig. 8. The XRD pattern of the corrosion products on the non-loaded hot corrosion specimen.

in the corrosion-product scale was independent of creep. In other words, C1 and the non-loaded specimen were hot-corroded similarly.

Fig. 7b and c depict creep cracks and the relevant X-ray maps of the specimen C1 after creep under at 850 °C. It is indicated that the salt coating melted and penetrated into the cracks and consequently led to aggressive hot corrosion. Hot corrosion inside the cracks also caused drastic internal oxidation and Cr depletion. By contrast, a thin protective monolayer oxide scale formed on the surface and inside the cracks of the specimen N1 (Fig. 7d). This Cr-rich scale, despite the longer exposure time of N1 (about 79 h) compared with C1 (about 45 h), protected Ni and Co against further oxidation; although it led to Cr depletion in the sub-surface zone.

The XRD analysis of corrosion products on the non-loaded specimen is shown in Fig. 8. Detection of Ni–Cr sulfides in corrosion products and considering the test temperature (850 °C) demonstrates that the predominant corrosion mechanism is of type I or High Temperature Hot Corrosion (HTHC) [11]. Through this type of hot corrosion, the Cr-rich protective oxide that forms on Alloy 617 at high temperature is corroded by fluxing in the fused salt. Therefore, the fused salt directly reaches the bare alloy and causes severe corrosion.

Alloy 617 contains a considerable amount of Mo which influences the corrosion behavior. Na_2MoO_4 was detected in the XRD pattern; it means that Mo had entered the fused salt and formed the corrosive liquid phase of Na_2SO_4–MoO_3. The presence of Na_2SO_4–MoO_3 in the fused salt leads to the alloy-induced acidic fluxing of Ni and consequently forms $NiMoO_4$ [11], as detected in XRD pattern. In addition, the presence of $NaVO_3$ in the salt mixture increased hot corrosion attack by enhancing the acidic solubility of Ni–Co oxides [12] and forming $Ni_3(VO_4)_2$ and $Co_3(VO_4)_2$.

The Ni, Cr and Co content of Alloy 617 formed various oxides (Fig. 8). These oxides are classified as the positive-type metal-deficit semiconductors and accordingly lead to the outward flux of cations from alloy to oxide. The outward cation flux leaves vacancies in the alloy adjacent to the alloy-oxide interface [11]. These generated vacancies have a significant role in the interaction of hot corrosion and creep.

During creep, the stress concentration in the alloy microstructure acts as a drive force to move the vacancies and condense them into vacancy sinks that are high stress regions at the transvers grain boundaries and particularly the triple points. The condensed vacancies then change into voids [13]. In addition, grain boundary oxidation promoted by intergranular $M_{23}C_6$ precipitates increases the voids in farther depth. Considering the hot corrosion role, it is stated that hot corrosion accelerates the ionic migration (cation flux) throughout the alloy-scale interface, which results in the formation of more and larger grain boundary voids.

All the void-formation phenomena explained above generate voids that act as suitable sites for creep-crack initiation. These voids also join the cavities formed by plastic deformation during creep to reach the critical size necessary for propagation. As a result, tertiary creep stage starts earlier under hot-corrosion (as observed in Fig. 3), which is attributed to the reduction of incubation time for creep-crack initiation.

It is further stated that the additional voids formed by hot corrosion enhance “the rate of cavity formation with strain” and consequently reduce the strain-to-rupture [13]; see Fig. 3.

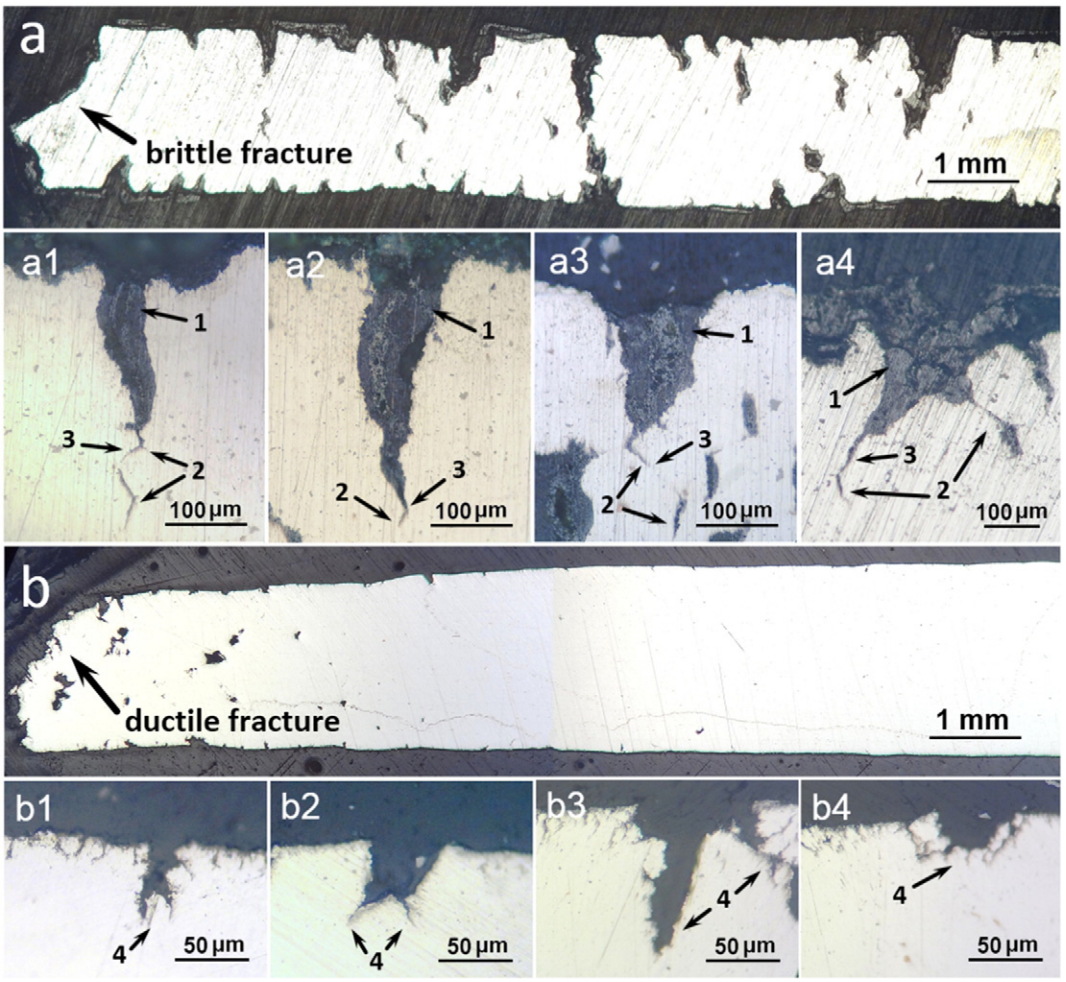

Fig. 9. Optical micrographs of surface cracks in (a) C1 and (b) N1; **1**: fused-salt penetration into cracks; **2**: grain boundary hot corrosion and oxidation; **3**: crack sharpening; **4**: crack branching.

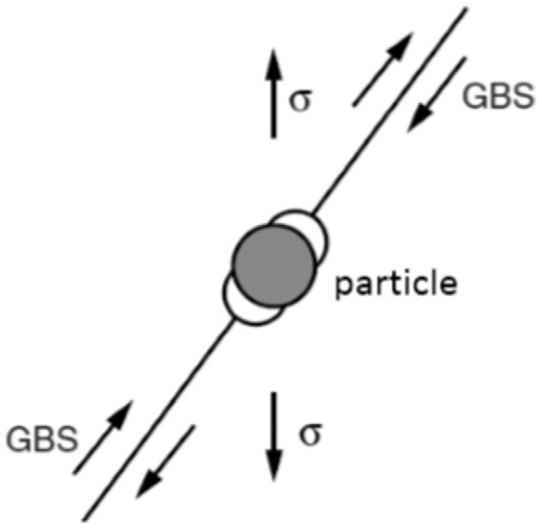

Fig. 10. Formation of a cavity from a particle-obstacle (i.e. an oxide particle) in conjunction with grain boundary sliding (GBS) [13].

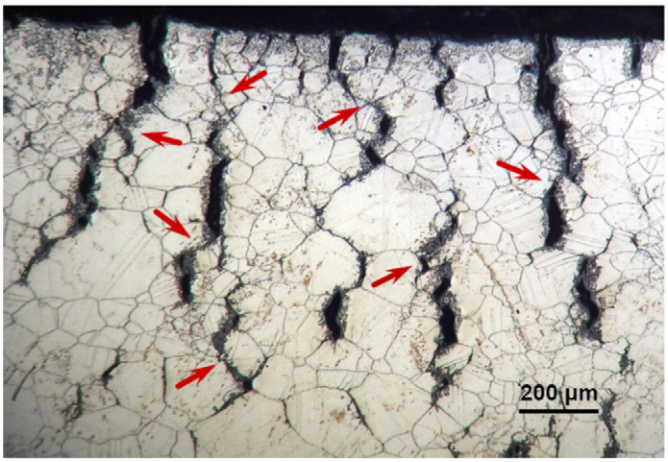

Fig. 11. Optical micrograph of C1 in the longitudinal section, demonstrating damage accumulation.

Fig. 9 compares the crack morphology in the ruptured specimens C1 and N1. As indicated in Fig. 9a, the penetration of the fused salt into cracks caused the cracks to grow severely in addition to deeper grain boundary oxidation ahead of cracks. Extensive oxidation in front of the crack tip (indicated by number 2) raises the phenomenon of Stress-Accelerated Grain-Boundary Oxidation (SAGBO), which proposes that oxygen diffuses into grain boundaries through stress-assisted diffusion [14].

SAGBO leads to the formation of intergranular oxide particles. These particles act as creep-crack nucleation-sites [13] since they are obstacles to the grain boundary sliding and produce stress concentration due to their incoherency with the crystal structure. The nucleation of cracks from oxide particles (Fig. 10) is assumed to promote grain-boundary "direct decohesion" during tertiary regime.

The fused salt, present in cracks during creep, prevents micro-branches of cracks from growing by dissolving them immediately after nucleation. Therefore, cracks cannot distribute stress among branches, which increases stress concentration ahead of the crack tip and ultimately enlarges and sharpens cracks. The crack sharpening, indicated by number 3 in Fig. 9a, also demonstrates that the cracks in C1 experienced rapid growth rate. The sharper and larger cracks in the salt-coated specimens partly explains the decrease in strain-to-rupture (cf. Fig. 3) and the percentage of reduction in area (cf. Table 3). By contrast, without hot corrosion (Fig. 9b), crack branches distributed stress and strain more uniformly along the gage and retained the ductility.

During simultaneous hot corrosion and creep, the alloy chemical composition changes locally at the grain boundaries due to the phenomena of outward cation migration, Cr depletion, grain boundary oxidation and the penetration of corrosive species (from the fused salt) into intergranular cracks. These chemical changes lead the grain boundary cohesive strength to decrease, as also discussed by [5,15]. In this way, hot corrosion facilitates grain-boundary direct decohesion and thus accelerates rupture. The direct decohesion of boundaries leads to extensive cavitation at transverse boundaries, as shown in Fig. 11. It should be noted here that, meanwhile, grain-boundary sliding/migration (the other creep mechanism) also progresses.

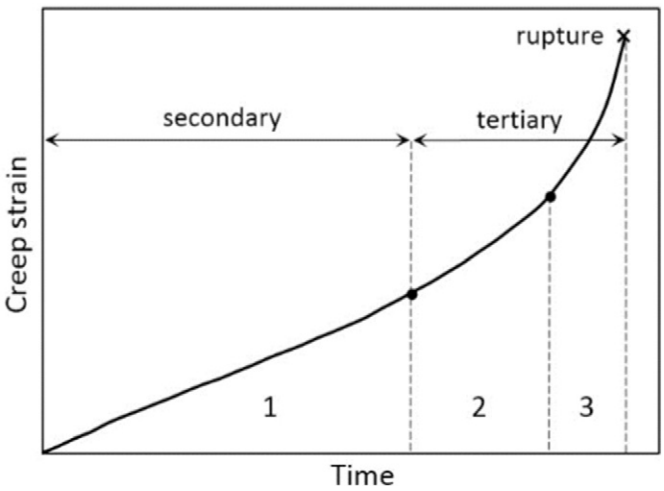

Fig. 12. Stages of the interaction between hot corrosion and creep; **1**: degrading the alloy creep properties by hot corrosion and scale cracking by creep deformation; **2**: damage accumulation, hot corrosion in surface cracks and grain-boundary decohesion/sliding; **3**: creep rupture.

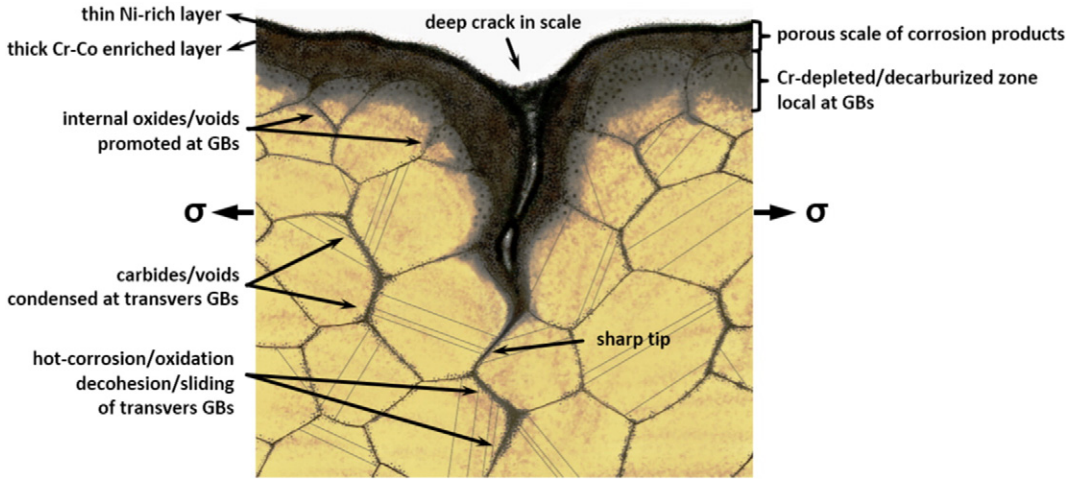

Fig. 13. Schematic view of the surface crack generated by the interaction between hot corrosion and creep.

The damage by hot corrosion and creep cavities accumulates at grain boundaries during creep and then erupts as tertiary creep commences. Thus, the interaction takes effect largely in the tertiary stage. Damage accumulation (indicated in Fig. 11) is a significant interaction mechanism via which coalescence/inter-linkage of cavities and cracks occurs and large grain boundary cracks form, grow rapidly and finally cause early rupture.

It is stated that volatile species such as Ni–Cr chlorides [5,11] and MoO_3 [3] formed in the fused salt respectively due to the presence of NaCl in the salt and Mo in Alloy 617. These species change into gas and leave cracks in the scale (cf. Fig. 5a). Additionally, during creep under simultaneous hot corrosion, the corrosion-product scale cracks frequently owing to the rapid strain particularly in tertiary creep. The cracks in scale provide more and shorter paths for the air to introduce oxygen into the fused salt, which sustains the corrosive nature of salt and also diffuses oxygen into the alloy along the grain boundaries. As Jang et al. [16] explained, the diffusion of oxygen along grain boundaries exposes Alloy 617 to further decarburization that takes place at 850 °C. Decarburization facilitates grain-boundary sliding by depleting the intergranular carbides that could limit boundary motion. However, owing to the limited depth of hot corrosion and decarburization, it is not alleged that they change the predominant rupture mechanism. This is consistent with the observation of Swaminathan and Raghavan [3] which indicates that the rupture activation-energy of Alloy C-276 does not considerably change under vanadic attack.

Considering all the observations and discussions in the present work, a typical creep curve is given in Fig. 12 to clarify when each interaction mechanism takes place. This curve includes 3 stages and involves secondary and tertiary creep stages. In the first stage, hot corrosion gradually degrades the creep properties of the alloy and creep deformation frequently cracks the corrosion-product scale. The second stage includes damage accumulation, hot corrosion in surface cracks and grain-boundary decohesion and sliding. As these mechanisms progress, the alloy reaches its critical level of strain that leads to rupture in the third stage. In fact, practically, there is no distinguishable boundary between interaction stages, and mechanisms of each stage may continue through the next stages.

Fig. 13 represents a schematic view of the surface cracks generated by the interaction with the relevant characteristics discussed previously. This schema corresponds to the situation in which Alloy 617 is simultaneously subjected to rapid grain-boundary creep and HTHC in sodium salts. In such situations, hot-corrosion and oxidation synergistically join with the stress concentration around cracks to localize the damage efficiently at the crack tip. They subsequently promote boundary decohesion and sliding, which ultimately leads to premature rupture.

4. Conclusion

The objective of this study was to investigate more details of the interaction of hot corrosion and creep. The main results are concluded as the followings:

- At 850 °C, the HTHC of Alloy 617 in sodium salts results in a drastic reduction of the creep life. First, hot corrosion enhances the secondary-creep rate and leads to the early start of tertiary creep by increasing intergranular oxides and voids, which degrades the alloy creep properties. Subsequently, hot corrosion in cracks promotes SAGBO, thereby accelerating creep-crack propagation. Finally, damage accumulation enhances rupture process during tertiary creep. The reduction in load-bearing cross section by hot corrosion does not considerably affect the creep behavior.
- Intergranular $M_{23}C_6$ precipitates are substantially involved in the destructive effects of hot corrosion and enhance hot-corrosion/creep interaction.

- Hot corrosion increases the cavity-nucleation rate and restrains crack branching and the uniform distribution of stress and strain. In addition, damage accumulation generates large cracks. These all lead to the brittle creep-behavior of alloy.
- Hot corrosion enables grain-boundary direct decohesion during tertiary creep as it generates numerous intergranular oxide particles and decreases grain-boundary cohesive-strength. On the other hand, decarburization which is promoted by hot corrosion and creep, enhances the grain-boundary sliding.
- Creep does not change the hot corrosion mechanism and only intensifies it at grain boundaries by opening the cracks and condensing carbides and voids at grain boundaries.

Acknowledgment

The authors acknowledge the financial support of Institute of Science and High Technology and Environmental Sciences (7/5948) and Kerman Combined Cycle Power Plant (93/39) and also wish to thank Dr. M. Hajizamani for providing language help.

References

[1] W. Ren, R. Swindeman, A review on current status of Alloys 617 and 230 for gen IV nuclear reactor internals and heat exchangers, Press. Vessel Tech. 131 (2009) 044002-1–044002-15.
[2] H. Singh, D. Puri, S. Prakash, An overview of Na_2SO_4 and/or V_2O_5 induced hot corrosion of Fe- and Ni-based superalloys, Material Science 16 (2007) 27–50.
[3] J. Swaminathan, S. Raghavan, Vanadic hot corrosion-creep interaction of superni-C276 in the temperature range 650–750 °C, High Temp. Mater. Process. 13 (1994) 277–297.
[4] T.L. Lin, Y.H. Zhang, H.W. Yang, Influence of hot corrosion on the creep strength of the nickel-base superalloy GH37, Mater. Sci. Eng. 62 (1984) 17–24.
[5] V. Suryanarayanan, K.J.L. Iyer, V.M. Radhakrishnan, Interaction of low temperature hot corrosion and creep, Mater. Sci. Eng. A112 (1989) 107–116.
[6] M. Yoshiba, The role of applied creep stress on hot corrosion behavior of a nickel-base superalloy, High Temperature Corrosion of Advanced Materials and Protective Coatings (1992) 187–196.
[7] J.K. Solberg, H. Thon, Creep/Corrosion of two nickel alloys in combustion gas, Metallurgical Transactions, 14a (1983) 1213–1221.
[8] N. Roy, R.N. Ghosh, M.C. Pandey, Modelling of interaction between creep and oxidation behaviour for engineering materials, ISIJ Int. 41 (2001) 915–921.
[9] S. Chomette, J.-M. Gentzbittel, B. Viguier, Creep behavior of as received, aged and cold worked Inconel 617 at 850 °C and 950 °C, J. Nucl. Mater. 399 (2010) 266–274.
[10] W. Qiong, L. Shu-Suo, M. Yue, G. Sheng-Kai, First principles calculations of alloying element diffusion coefficients in Ni using the five-frequency model, Chin. Phys. B. 21 (2012) 109102-1–109102-7.
[11] N. Birks, G.H. Meier, F.S. Pettit, Introduction to the High-Temperature Oxidation of Metals, second ed. Cambridge University Press, 2006.
[12] R.A. Rapp, Hot corrosion of materials: a fluxing mechanism? Corros. Sci. 44 (2002) 209–221.
[13] M.E. Kassner, Fundamentals of creep in metal and alloys, second ed., Elsevier, 2009.
[14] X. Liu, B. Kang, W. Carpenter, E. Barbero, Investigation of the crack growth behavior of inconel 718 by high temperature Moiré interferometry, Mater. Sci. 39 (2004) 1967–1973.
[15] B. Pieraggi, Effect of creep or low cycle fatigue on the oxidation or hot corrosion behaviour of nickel-base superalloys, Mater. Sci. Eng. 88 (1987) 199–204.
[16] C. Jang, D. Lee, D. Kim, Oxidation behaviour of an Alloy 617 in very high-temperature air and helium environments, Int. J. Press. Vessel. Pip. 85 (2008) 368–377.